

# Polymeric Behaviour of DNA: Theta Temperature and Good Solvent Cross-over of Gyration and Hydrodynamic Radii

Sharadwata Pan,<sup>1,2,3</sup> P. Sunthar,<sup>2,1</sup> T. Sridhar,<sup>3,1</sup> and J. Ravi Prakash<sup>3,1,a)</sup>

<sup>1)</sup>IITB-Monash Research Academy, Indian Institute of Technology Bombay, Powai, Mumbai - 400076, India

<sup>2)</sup>Department of Chemical Engineering, Indian Institute of Technology Bombay, Powai, Mumbai - 400076, India

<sup>3)</sup>Department of Chemical Engineering, Monash University, Melbourne, VIC 3800, Australia

(Dated: 11 May 2019)

The radius of gyration and the hydrodynamic radius of a number of linear, double-stranded DNA molecules, ranging in length from 3 to 300 kilobase pairs, extracted from modified strains of *E. coli* and dissolved in the presence of excess salt in two commonly used solvents, have been obtained by static and dynamic light scattering measurements. Using scaling relations from polymer solution theory, the  $\theta$ -temperature in each of the solvents, and the crossover swelling of the two radii have been determined. It is shown that, as in the case of neutral synthetic polymer solutions, DNA solutions exhibit universal behaviour that can be described by the two-parameter theory.

PACS numbers: 61.25.he, 82.35.Lr, 83.80.Rs, 87.14.gk, 87.15.hp, 87.15.N-, 87.15.Vv

Keywords: Dilute polymer solution; excluded volume interactions; static and dynamic scaling; DNA solution

## I. INTRODUCTION

DNA is a polyelectrolyte, but under high salt conditions behaves like a charge neutral worm-like chain<sup>1–5</sup> with a persistence length of about 50 nm<sup>6</sup>. The monodispersity of DNA and its ability to be stained for visualization has made it an excellent candidate for studying the static and dynamic properties of polymer solutions<sup>7</sup>, both at and far from equilibrium and at a range of concentrations<sup>2–4,8–23</sup>. For instance, experimental measurements have been carried out of diffusivity<sup>4,13,24–28</sup>, intrinsic viscosity<sup>22,23</sup>, relaxation times in semi-dilute solutions<sup>29,30</sup>, extensional viscosity<sup>10</sup> and conformational evolution in cross slot flows<sup>31,32</sup>. In all these experimental observations, it is implicitly assumed that DNA solutions in excess salt are identical in their behaviour to neutral polymer solutions. Indeed all experimental observations so far support this implicit assumption in terms of general expectations of their behaviour. However, a unique aspect of solutions of synthetic polymers of sufficiently large molecular weight, namely, the existence of universal behaviour due to the self-similar character of polymer molecules, has not been investigated for DNA solutions. Universal behaviour enables the representation of experimental observations in terms of master plots, and the description of solution behaviour in terms of scaling variables.

An example of universal behaviour that is of relevance to this work is that exhibited by the swelling of individual polymer chains when the polymer solution temperature  $T$  increases above the  $\theta$  temperature,  $T_\theta$ , due to repulsive intramolecular interactions. Such expansion is well described by dimensionless expansion (or swelling) ratios<sup>33</sup>, for in-

stance,  $\alpha_g$  for  $R_g$  and  $\alpha_H$  for  $R_H$ :

$$\alpha_g = \frac{R_g(T)}{R_g^\theta} \quad (1)$$

$$\alpha_H = \frac{R_H(T)}{R_H^\theta} \quad (2)$$

where,  $R_g(T)$  and  $R_H(T)$  are the radius of gyration and the hydrodynamic radius at any temperature  $T > T_\theta$ , and  $R_g^\theta$  and  $R_H^\theta$  represent the  $\theta$ -temperature values of these quantities. As is well known, while the scaling of the radius of gyration and the hydrodynamic radius with molecular weight  $M$  obeys universal power laws in the special cases of  $\theta$ , athermal, and non-solvents, in the intermediate crossover region between  $\theta$  and athermal solvents, the ratios  $\alpha_g$  and  $\alpha_H$  can be collapsed onto master plots when plotted in terms of a single scaling variable,  $\tau = \left(1 - \frac{T_\theta}{T}\right) \sqrt{M}$ , that combines the dependence on temperature and molecular weight<sup>34,35</sup>.

In the case of neutral synthetic polymer solutions, this universal behaviour is commonly interpreted in terms of the two-parameter theory<sup>36,37</sup>. According to the two-parameter theory, the values of properties at any temperature  $T$  under good solvent conditions, can be expressed as an unique function of just two parameters, namely, the radius of gyration under  $\theta$  conditions,  $R_g^\theta$ , and a solvent quality parameter, commonly denoted by  $z$ <sup>38</sup>. The parameter  $z$  is proportional to the square root of the number of monomers in the polymer chain, with the proportionality constant being related to the binary cluster integral, which reflects the chemistry of solvent-mediated interactions between monomers in different parts of the chain<sup>34,36</sup>. Thus, for instance,

$$R_g(T) = R_g^\theta f_g(z) \quad (3)$$

implying the universal two-parameter theory prediction,  $\alpha_g = f_g(z)$ , where  $f_g$  is a universal function of  $z$ , whose specific

<sup>a)</sup>Corresponding author: ravi.jagadeeshan@monash.edu

form will be elaborated later. Similar predictions are made by two-parameter theory for  $\alpha_H$  and the swelling of the viscometric radius  $R_v$ , which is based on the intrinsic viscosity<sup>35</sup>. The connection between universal two-parameter theory predictions and the master plots obtained by experiments on synthetic polymer solutions has been made by relating  $z$  to the scaling variable  $\tau$  through a simple linear relation  $z = k\tau$ , where  $k$  is a constant that depends on polymer-solvent chemistry<sup>35,38</sup>.

Away from equilibrium, a scaling variable in addition to  $z$  is required to characterize dilute solution behaviour. For instance in shear flows, it has been found that including a characteristic shear rate  $\beta$  enables the representation of rheological behaviour in terms of universal plots<sup>39,40</sup>, while in extensional flows, the inclusion of the Weissenberg number  $Wi$  enables a similar representation<sup>8</sup>. Indeed, a quantitative comparison of the stretch evolution of DNA in a cross slot flow<sup>9</sup>, and the extensional viscosity of DNA solutions in uniaxial elongational flow<sup>10</sup> was shown to be possible once an estimate of the solvent quality  $z$  of the solution was made. However, to the best of our knowledge, a systematic study to estimate the solvent quality of DNA solutions has not been attempted so far. The characterization of DNA solutions in terms of the two-parameter theory would provide a powerful predictive tool for theoretical analysis of its dynamics in equilibrium and in flow.

In this paper, we show that, similar to the behaviour exhibited by charge neutral synthetic polymer solutions, the swelling of DNA solutions in excess salt also exhibits universal behaviour in the context of two properties: (i) the swelling of  $R_g$ , which is a static equilibrium property, and (ii) the swelling of  $R_H$ , which is a dynamic equilibrium property. In order to do this, we first establish the  $\theta$ -temperature of two different DNA solutions, and use static and dynamic light scattering measurements to systematically characterize DNA molecules in an extended range of molecular weights from 3–300 kilobase pairs (kbp) ( $\approx 10^6$ – $10^8$  daltons).

The plan of the paper is as follows. In the next section, we briefly describe the protocol for our experiments, with details deferred to the supporting information. In section III A, the procedure adopted for determining the  $\theta$  temperature of DNA solutions is described. Section III B compares the persistence length of DNA measured here, with several earlier observations. In section III C, the swelling of DNA solutions is compared to the previously reported swelling of charge neutral synthetic polymers and to the results of prior predictions by Brownian dynamics simulations. The reliability of measurements under poor solvent conditions is examined from several different perspectives in section III D. Our conclusions are summarised in section IV.

## II. METHODOLOGY

In order to experimentally characterize the properties of double-stranded DNA, a range of large molecular weight DNA, each with a monodisperse population, is desirable. The present work is greatly facilitated by the work of Smith's group<sup>11</sup> who genetically engineered special double-stranded

DNA fragments in the range of 3–300 kbp and incorporated them inside commonly used *Escherichia coli* (*E. coli*) bacterial strains. These strains can be cultured to produce sufficient replicas of its DNA, which can be cut precisely at desired locations to extract the special fragments.

The *E. coli* stab cultures were procured from Smith's group and the DNA fragments were extracted, linearized and purified according to standard molecular biology protocols<sup>11,41</sup>. The various DNA fragments used here are listed in Table I of the supplementary material. Also given in the supplementary material are details of working conditions, procedures for preparation and quantification of linear DNA fragments, the methodology for preparing samples and carrying out dynamic and static light scattering measurements, and the approach used here for the determination of second virial coefficients. For each molecular weight, the purified linear DNA pellet was dissolved in two solvents denoted here as Solvent I (Tris-EDTA Buffer) and Solvent II (which is predominantly Sucrose). Both these solvents are commonly used in physics<sup>2,4,9</sup> and rheology<sup>10</sup> experiments. They contain 0.5 M NaCl, which we establish shortly below is above the threshold for observing charge-screening effects<sup>5</sup>. Consequently, the DNA molecules are expected to behave identically to neutral molecules. The detailed composition of both solvents is given in Table II of the supplementary material. We have used Static Light Scattering (SLS) (BI-200SM Goniometer, Brookhaven Instruments Corporation, USA) to determine  $R_g$  and the second virial coefficient  $A_2$  at different temperatures (from 10–35°C), and dynamic Light Scattering (DLS) (Zetasizer Nano ZS, Malvern, UK) has been employed to determine  $R_H$  at different temperatures (from 5–35°C). A concentration of  $c/c^* = 0.1$  (for DLS) and  $c/c^* = 0.05$ – $0.1$  (for SLS) has been used throughout this study. Note that,  $c^* = \frac{M}{N_A(4\pi/3)R_g^3}$ , is the overlap concentration, calculated based on the measured values of  $R_g$ , with  $N_A$  being the Avogadro number. Typical  $c^*$  values for different DNA molecular weights are listed in Table III of the supplementary material. Initial estimates of  $c^*$  were based on values of  $R_g$  suggested in Ref. 11 for molecular weights that are identical to those used in this study.

## III. RESULTS AND DISCUSSION

### A. Determination of the $\theta$ -temperature

In order to proceed with the experiments proposed in this work, it is essential to first establish the salt concentration regime in which DNA (a polyelectrolyte) behaves as a neutral polymer. We have measured the hydrodynamic radius of two different linear DNA fragments across a range of salt concentrations (from 0.001 to 1 M) at 25°C and the results are displayed Figure 1. It is clear from the figure that complete charge screening occurs above 10 mM NaCl. This is in agreement with earlier dynamic light scattering studies on linear DNA<sup>28,42,43</sup>. Since both the solvents used here contain 0.5 M NaCl, the light scattering experiments of the current study are in a regime well above the threshold for observing

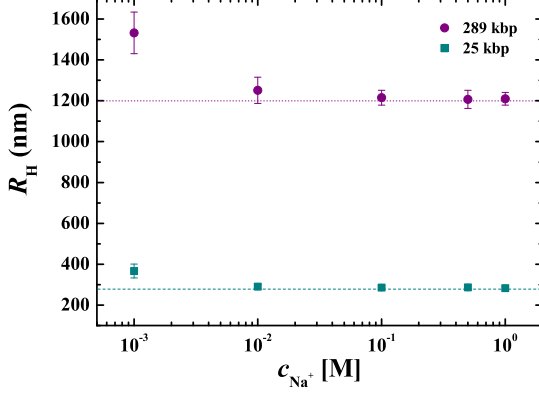


FIG. 1. Dependence of  $R_H$  on salt concentration for two different molecular weights at 25 °C.

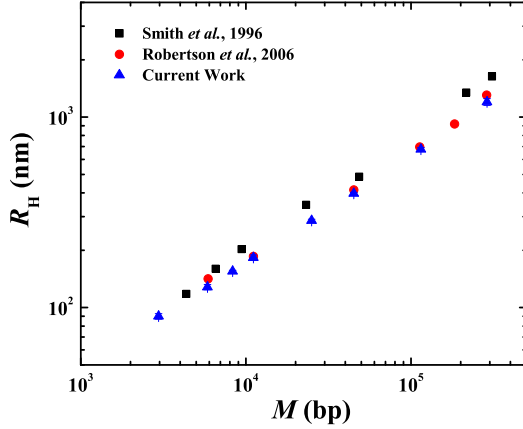


FIG. 2. Comparison of the molecular weight dependence of hydrodynamic radius, obtained previously by Smith, Perkins, and Chu<sup>2</sup> and Robertson, Laib, and Smith<sup>4</sup> at 25°C, with current measurements in Solvent I.

charge screening effects. We have also determined the persistence length of DNA under conditions where the charges are completely screened, and our estimate agrees with earlier measurements of the persistence length under such conditions. These results are discussed subsequently in section III B, since they require an estimate of the  $\theta$ -temperature.

Figure 2 compares present measurements of the dependence of hydrodynamic radius on molecular weight with previous measurements<sup>2,4</sup> at 25°C. While Smith, Perkins, and Chu<sup>2</sup> used fragments and concatenates of  $\lambda$  phage DNA to obtain molecules across the wide range of molecular weights that were studied, the measurements of Robertson, Laib, and Smith<sup>4</sup> were carried out on molecules identical to those that have been used here. These results were used by Smith and co-workers to demonstrate that double-stranded DNA in solutions with excess salt obey the molecular weight scaling ex-

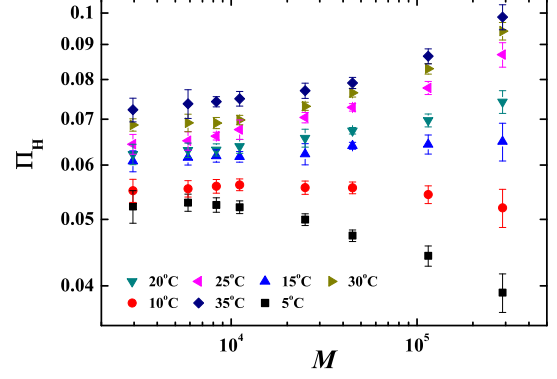


FIG. 3. Scaled hydrodynamic radius ( $\Pi_H$ ) as a function of molecular weight in base-pairs or bp (in Solvent I). Slopes are calculated at each temperature by a least-squares linear fit of the last four data points.

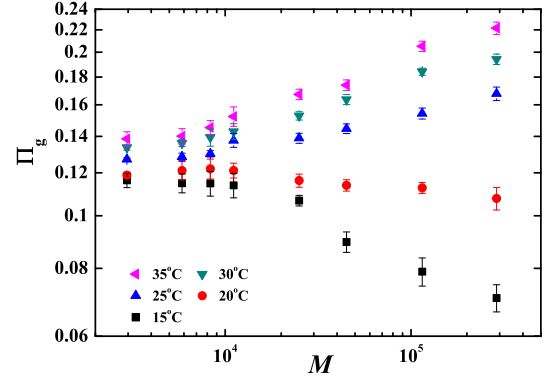


FIG. 4. Scaled radius of gyration ( $\Pi_g$ ) as a function of molecular weight in bp (in Solvent II). Slopes are calculated at each temperature by a least-squares linear fit of the last four data points.

pected from polymer solution theory in the presence of excluded volume interactions. In the present work, we extend the measurements to a wide range of temperatures in order to carry out a systematic study of the crossover region between  $\theta$  and very good solvents.

The  $\theta$ -temperature for a particular polymer-solvent pair can be inferred from the measured data, by several signatures. We have employed two methods—molecular weight scaling and the second virial coefficient transition. At the  $\theta$ -temperature,  $R_g$  and  $R_H$  scale as  $M^{0.5}$  for large molecular weight linear polymers. With this expected behaviour, two dimensionless

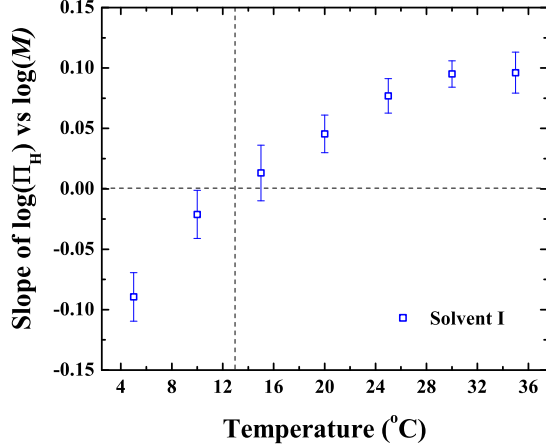


FIG. 5. Variation of slope obtained from Figure 3 with temperature (in Solvent I). Readings corresponding to 5 to 25°C are fitted with a second order polynomial to calculate the  $\theta$ -temperature.

scaling variables can be defined:

$$\Pi_g \equiv \frac{R_g}{a \sqrt{M}} \quad (4)$$

$$\Pi_H \equiv \frac{R_H}{a \sqrt{M}} \quad (5)$$

where,  $a$  is a constant with dimensions of length, which we have set equal to 1 nm. Both  $\Pi_H$  and  $\Pi_g$  should increase with molecular weight for good solvents, remain constant for theta solvents, and decrease for poor solvents.

Figures 3 and 4 show  $\Pi_H$  and  $\Pi_g$  plotted against  $M$  in log-log plots, for solvents I and II, respectively. In line with expectation, the data shows a monotonic trend: decreasing with molecular weight for certain temperatures, remaining relatively constant at intermediate temperatures, and increasing with  $M$  for higher temperatures. In order to determine the  $\theta$ -temperature precisely, the *effective* slope of the curves at sufficiently large molecular weights was plotted against absolute temperature and fitted either with a second order polynomial or subjected to linear interpolation. The temperature where the sign of the slope changes from negative to positive, is taken to be  $T_\theta$ . A value of  $T_\theta = 13 \pm 2$  °C was estimated for DNA-Solvent I, after taking into account experimental errors in  $\Pi_g$  or  $\Pi_H$  (see Figure 5). A similar procedure for Solvent II leads to  $T_\theta = 23 \pm 2$  °C.

Figures 3 and 4 also indicate that for the relatively *smaller* molecular weight samples, at all the observed temperatures, both  $\Pi_H$  and  $\Pi_g$  are roughly constant with increasing molecular weight. This behaviour is consistent with the *blob* scaling argument which anticipates that below a length scale corresponding to a *thermal blob*, the energy of excluded volume interactions is less than  $k_B T$  (where  $k_B$  is the Boltzmann constant), as a result of which chain segments with size less than the blob size obey ideal chain statistics, and scale as  $M^{0.5}$  at all

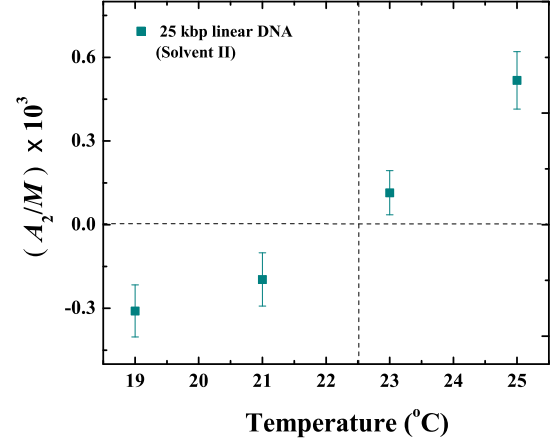


FIG. 6. Variation with temperature of the ratio of second virial coefficient to molecular weight, in Solvent II. Data points are fitted with a second order polynomial to calculate the  $\theta$ -temperature.

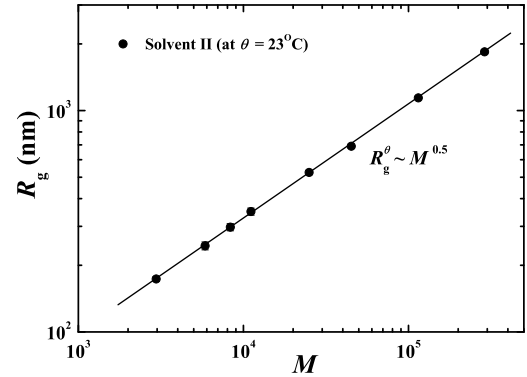


FIG. 7. The variation of the radius of gyration ( $R_g$ ) with molecular weight (in bp) at 23°C, which is estimated to be the  $\theta$ -temperature for Solvent II.

temperatures<sup>34</sup>. In section III D, we exploit the consequences of this scaling argument to determine the size of thermal blobs as a function of temperature in DNA solutions, under good and poor solvent conditions.

An alternative method employed in synthetic polymer literature for estimating the theta temperature is by determining the second virial coefficient  $A_2$ <sup>44–46</sup>, either from the concentration dependence of osmotic pressure, light scattering from dilute polymer solutions, or by measuring intrinsic viscosities of dilute polymer solutions.  $A_2$  is a direct measure of excluded volume interactions between pairs of chains<sup>34</sup>. In this work, a quantity that is linearly proportional to the second virial coefficient is determined for a single, linear, medium molecular weight DNA fragment (25 kbp) by static light scattering,

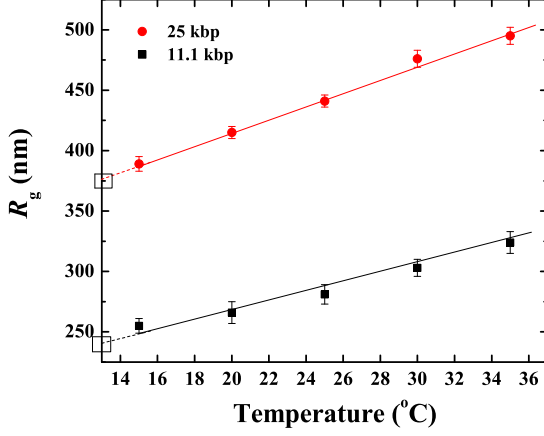


FIG. 8. Estimation of  $R_g^\theta$  by extrapolation of  $R_g$  values measured at various temperatures to the value of  $T_\theta = 13^\circ\text{C}$ , for two different molecular weights, in Solvent I.

according to the procedure described in Ref. 45. The exact values of  $A_2$  are not determined since we are interested only in the temperature where it vanishes. The sign of  $A_2$ , which is indicative of repulsion or attraction between the segments of a chain<sup>34</sup>, is positive in good solvents, negative in a poor solvents and vanishes at the theta temperature. The temperature at which  $A_2$  vanishes, determined by interpolating the measured data, is used here as an estimate of  $T_\theta$ , as shown in Fig. 6 for Solvent II. We find  $T_\theta = 13 \pm 2^\circ\text{C}$  for Solvent I, and  $T_\theta = 22.5 \pm 1^\circ\text{C}$  for Solvent II. These values agree, within experimental error, with the values obtained using the molecular weight scaling method.

Once the values of  $T_\theta$  in the two solvents have been determined, the values of  $R_g^\theta$  for all the molecular weights considered here can be evaluated from values of  $R_g$  measured at the various temperatures. In the case of solvent II, since  $T_\theta$  lies within the range of experimental temperatures,  $R_g^\theta$  can be obtained by linear interpolation. The values of  $R_g^\theta$  determined by this procedure are plotted against  $M$  in Fig. 7, which confirms that indeed ideal chain statistics are obeyed at the estimated  $\theta$ -temperature for Solvent II. In the case of Solvent I, the values of  $R_g^\theta$  at different molecular weights have been evaluated here by linearly extrapolating values of  $R_g$  measured at a fixed molecular weight and different temperatures  $T > T_\theta$ , to the value of  $T_\theta$ . Figure 8 demonstrates this procedure for two different molecular weights, using values of  $R_g$  measured at various temperatures. Estimated values of  $R_g^\theta$  for all the molecular weights considered here, in both Solvents I and II are listed in Tables VI and VII of the supplementary material.

## B. Estimation of the persistence length

At the  $\theta$ -temperature, since a polymer chain obeys Gaussian statistics, the persistence length  $P$  is related to the radius

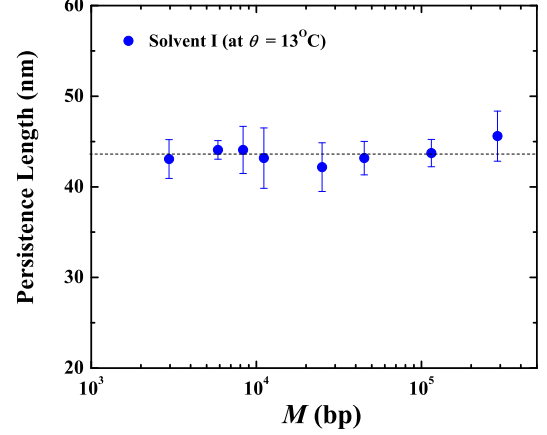


FIG. 9. Molecular weight independence of DNA persistence length.

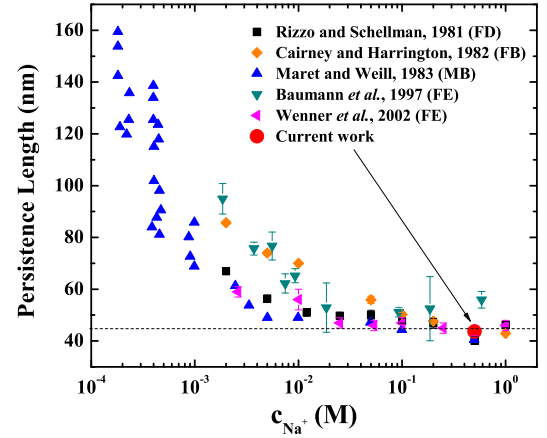


FIG. 10. Dependence of DNA persistence length on salt concentration, collated from data reported previously. The DNA molecular weights used in all these studies range from 3–300 kbp. The mean persistence length for all the molecular weights shown in Figure 9 is denoted here by the opaque red circle. Abbreviations: ‘FD’ - Flow Dichroism, ‘FB’ - Flow Birefringence, ‘MB’ - Magnetic Birefringence, ‘FE’ - Force Extension using optical tweezers.

of gyration  $R_g^\theta$  and the contour length  $L$ , through the relation  $P = 3(R_g^\theta)^2/L$ . In the asymptotic limit  $(R_g/L) \ll 1$ , this relationship is also valid for a worm-like chain. The persistence lengths evaluated using this expression, at the  $\theta$ -temperature for Solvent I, from known values of  $R_g^\theta$  and  $L$ , are shown in Figure 9. It is evident from the figure that the persistence length of DNA at a salt concentration of 0.5 M ( $\text{Na}^+$ ) is constant across all the molecular weights, with a mean value that is approximately 44 nm.

The effects of salt concentration on the persistence length of DNA has been studied earlier through a variety of techniques such as Flow Dichroism<sup>48</sup>, Flow Birefringence<sup>49</sup>, Magnetic Birefringence<sup>50</sup> and force-extension experiments using opti-

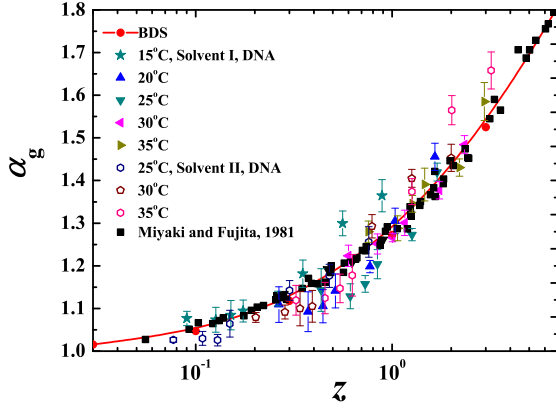


FIG. 11. Swelling of  $R_g$  vs  $z$ . The filled and open coloured symbols represent experimental data for DNA in Solvent I and II, respectively. BDS refers to the predictions of Brownian dynamics simulations,<sup>47</sup> with the curve representing the function  $f_g(z)$ , with constants  $a = 9.528$ ,  $b = 19.48$ ,  $c = 14.92$ , and  $m = 0.1339$ . Black squares represent experimental data of polystyrene in cyclohexane and benzene, reproduced from Miyaki and Fujita, 1981<sup>37</sup>.

cal tweezers<sup>51,52</sup>. Data from a number of these studies has been collated in Figure 10, with the mean value measured in the present study included. Clearly, the persistence length in all the earlier studies appears to reach an approximately constant value of 45-50 nm for salt concentrations  $> 0.1$  M, suggesting that the charges have been fully screened in this concentration regime. Both the value of the persistence length in the high salt limit, and the threshold concentration for charge screening obtained in this work are consistent with earlier observations.

Some early studies of the ionic dependence of DNA persistence length<sup>53-55</sup>, investigated via light scattering, have shown a strong dependence of persistence length on salt concentration even up to 4 M. Notably, these measurements were not at the  $\theta$ -temperature, and consequently, required both an estimation of the solvent quality, and a correction to account for excluded volume effects. The excluded volume corrections applied in the original papers were modified in subsequent studies<sup>56-58</sup>. These aspects might explain the differences observed from the present study, where both diffusivity and persistence length measurements suggest that charge screening is complete above 10 mM NaCl.

### C. The universal swelling of DNA

In order to establish the universal nature of the swelling of DNA molecules in solution, it is sufficient to show that the data in the crossover region between  $\theta$  and athermal solvents can be collapsed onto master plots when represented in terms of the scaling variable  $\tau$ . However, it is perhaps more useful for future comparisons between theories and experimental observations for DNA solution behaviour, if universal behaviour is established in a framework that enables such a comparison. As discussed earlier in section I, carrying out a systematic

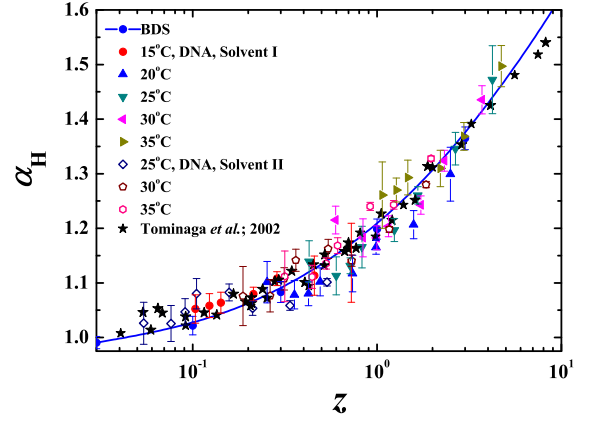


FIG. 12. Swelling of  $R_H$  vs  $z$ . The filled and open coloured symbols represent experimental data for DNA in Solvent I and II, respectively. BDS refers to the predictions of Brownian dynamics simulations<sup>59</sup>, with the curve representing the function  $f_H(z)$ , with constants  $a = 9.528$ ,  $b = 19.48$ ,  $c = 14.92$ , and  $m = 0.067$ . Black stars represent several experimental data on synthetic polymers collated in Tominaga *et al.*<sup>60</sup>.

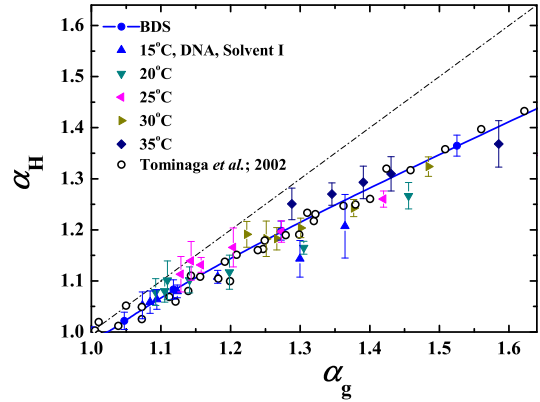


FIG. 13. Comparison of measured values of  $\alpha_H$  against  $\alpha_g$ . Filled symbols represent experimental data for DNA in Solvent I at good solvent conditions ( $T > T_\theta$ ). BDS refers to the predictions of Brownian dynamics simulations<sup>59</sup>. Open circles represent several experimental data on synthetic polymers collated in Tominaga *et al.*<sup>60</sup>.

comparison of experimentally determined expansion factors with the predictions of two-parameter theory requires relating the scaling variable  $\tau$  to the solvent quality parameter  $z$ , since theoretical predictions are made in terms of  $z$ .

Many versions of the two-parameter theory can be used for the purpose of comparison with experimental data. Early versions of the two-parameter theory, including Flory type *fifth power* theories, and theories based on perturbation expansions, are reviewed in the classic textbook by Yamakawa<sup>36</sup>. The use of two-parameter theory to describe numerical results on self-avoiding walks on lattices is reviewed in Ref. 61. While quantitative agreement between experiments and theory for the swelling of static properties such as the radius of

gyration  $R_g$  can be obtained with the help of renormalization group theories<sup>38</sup>, similar agreement has not been achieved for the swelling of the dynamic property  $R_H$  within this framework. Recently, quantitative predictions of both  $\alpha_g$  and  $\alpha_H$  have been achieved through the use of Brownian dynamics simulations<sup>47,59</sup>. These simulations, which make use of a narrow Gaussian potential to represent excluded volume interactions (that enables controlled simulations in terms of the parameter  $z$ ), give rise to parameter free predictions, independent of finite size effects, since they are based on the extrapolation of finite chain results to the long chain limit. In particular, the quantitative prediction of  $\alpha_H$  was shown to require the inclusion of fluctuating hydrodynamic interactions<sup>59</sup>. Interestingly, it turns out that lattice simulations, predictions of renormalization group theory, and results of Brownian dynamics simulations for the swelling of any typical generic property, say  $\alpha$ , can be described by universal functions that have the functional form  $\alpha = f(z)$ , where,  $f(z) = (1 + az + bz^2 + cz^3)^{m/2}$ , with the values of the constants  $a, b, c, m$  etc., dependent on the particular theory adopted<sup>38,47,62</sup>. Here, we choose to compare experimental results for  $\alpha_g$  and  $\alpha_H$  with the results of Brownian dynamics simulations, since they represent exact numerical simulations, and are not based on approximations unlike earlier analytical theories. The values of the various constants in the functions  $f_g$  and  $f_H$  that fit the results of Brownian dynamics simulations, are reported in the captions to Figs. 11 and 12.

The chemistry dependent constant  $k$  that relates the value of  $z$  in Brownian dynamics simulations to the experimental value of  $\tau$  remains to be determined. This is done as follows. Consider  $\alpha_g^{\text{expt}}$  to be the experimental value of swelling at a particular value of temperature  $T$  and molecular weight  $M$ . It is then possible to find the Brownian dynamics value of  $z$  that would give rise to the same value of swelling, from the expression  $z = f_g^{-1}(\alpha_g^{\text{expt}})$ , where  $f_g^{-1}$  is the inverse of the function  $f_g$ . Since  $z = k\hat{\tau}\sqrt{M}$ , where  $\hat{\tau} = \left(1 - \frac{T_\theta}{T}\right)$ , it follows that a plot of  $f_g^{-1}(\alpha_g^{\text{expt}})/\sqrt{M}$  versus  $\hat{\tau}$ , obtained by carrying out the same procedure for a number of values of  $T$  and  $M$ , would be a straight line with slope  $k$ . Once the constant  $k$  is determined, both experimental measurements of swelling and results of Brownian dynamics simulations can be represented on the same plot. As discussed in greater detail in the supplementary material, by using  $\theta$ -temperatures of 13°C and 23°C for Solvent I and II, respectively, the values of  $k$ , found by this procedure are  $7.4 \times 10^{-3} \pm 3.0 \times 10^{-4}$  for Solvent I and  $5.5 \times 10^{-3} \pm 2.0 \times 10^{-4}$  for Solvent II.

Experimental measurements and Brownian dynamics simulations predictions of the solvent quality crossover of the swelling of two measures of polymer size,  $\alpha_g$  and  $\alpha_H$ , are shown in Figs. 11 and 12. Experimental data of Miyaki and Fujita<sup>37</sup> and Tominaga *et al.*<sup>60</sup>, which are considered to be highly accurate measurements of synthetic polymer swelling, are also plotted alongside. An alternative,  $z$  independent, means of presenting the swelling data is displayed in Fig. 13, where the values of  $\alpha_g$ , at particular values of  $T$  and  $M$ , are plotted versus  $\alpha_H$  at the same values of  $T$  and  $M$ . From these figures it is evident that, just as in the case of synthetic poly-

mer solutions, irrespective of solvent chemistry, DNA solutions exhibit universal crossover behaviour from theta to good solvents.

#### D. Thermal blobs and measurements in poor solvents

The focus of the present paper is twofold, (i) determining the  $\theta$ -temperature, and (ii) describing the  $\theta$  to good solvent crossover behaviour in two different solutions of double-stranded DNA. The analysis of molecular weight scaling under poor solvent conditions has been carried out essentially only in order to locate the  $\theta$ -temperature. As is well known, the experimental observation of single chains in poor solvents is extremely difficult because of the problem of aggregation due to interchain attraction. Nevertheless, in this section we show that a careful analysis of the data displayed in Figs. 3 and 4, in the light of the blob picture, enables us to discuss the reliability of the measurements that have been carried out here under poor solvent conditions.

According to the blob picture of dilute polymer solutions, a polymer chain in a good or poor solvent can be considered to be a sequence of thermal blobs, where the thermal blob denotes the length scale at which excluded volume interactions become of order  $k_B T$ <sup>34</sup>. Under good solvent conditions, the blobs obeying self-avoiding-walk statistics, while they are space filling in poor solvents. As a result, the mean size  $R$  of a polymer chain is given by<sup>34</sup>,

$$R = R_{\text{blob}}(T) \left( \frac{N_k}{N_{\text{blob}}(T)} \right)^\nu \quad (6)$$

where,  $N_k$  is the number of Kuhn-steps in a chain,  $N_{\text{blob}}$  is the number of Kuhn-steps in a thermal blob, and  $R_{\text{blob}}$  is the mean size of a thermal blob. The Flory exponent  $\nu$  is 0.59 in a good solvent, and 1/3 in a poor solvent. The size of the thermal blob is a function of temperature. For instance, under athermal solvent conditions, the entire chain obeys self avoiding walk statistics, so the blob size is equal to the size of a single Kuhn-step. On the other hand, for temperatures approaching the  $\theta$ -temperature, the blob size grows to engulf the entire chain. From the definitions of  $\Pi_H$  and  $\Pi_g$  (see Eqs. (4)), it is clear that on length scales smaller than the blob length scale both these quantities must remain constant. On the other hand, Eq. (6) suggests that on length scales large compared to the blob length scale,  $\Pi_H$  and  $\Pi_g$  must scale as  $M^{0.09}$  in good solvents, and  $M^{-1/6}$  in poor solvents. Figure 14 re-examines the  $\log \Pi_H$  versus  $\log M$  data for Solvent I in the light of these arguments. It is clear that after an initial regime of constant values, there is a crossover to the expected scaling laws in both the good and poor solvent regimes. Similar behaviour is observed for Solvent II, and for the  $\log \Pi_g$  versus  $\log M$  data in both solvents (not shown here). The crossover from one scaling regime to the next begins approximately at the blob length scale, an estimate of which can be made as follows.

The requirement that the energy of excluded volume interactions within a thermal blob are of order  $k_B T$  leads to the



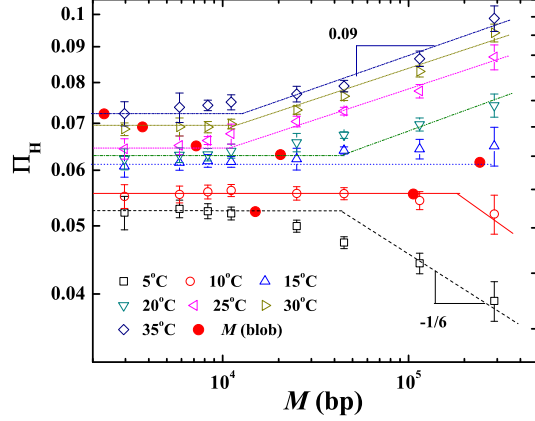


FIG. 14. Different scaling regimes for the scaled variable  $\Pi_H$  as a function of molecular weight  $M$ . The filled red circles correspond to the molecular weight  $M_{\text{blob}}$  of the chain segment within a thermal blob.

following expressions for  $N_{\text{blob}}$  and  $R_{\text{blob}}$ <sup>34</sup>,

$$N_{\text{blob}}(T) = \frac{b_k^6}{v(T)^2} \quad (7)$$

$$R_{\text{blob}}(T) = \frac{b_k^4}{|v(T)|} \quad (8)$$

where,  $b_k$  is the length of a Kuhn-step, and  $v(T)$  is the excluded volume at temperature  $T$ . The excluded volume can be shown to be related to the temperature through the relation,

$$v(T) = \begin{cases} v_0 \left(1 - \frac{T_\theta}{T}\right) & \text{for good solvents,} \\ -v_0 \left(1 - \frac{T}{T_\theta}\right) & \text{for poor solvents.} \end{cases} \quad (9)$$

where,  $v_0$  is a chemistry dependent constant. These expressions are consistent with the expectation that  $v \rightarrow v_0$  in an athermal solvent ( $T \rightarrow \infty$ ), and  $v \rightarrow -v_0$  in a non-solvent ( $T \rightarrow 0$ )<sup>34</sup>. Since measurements of the mean size (via  $R_g$  and  $R_H$ ) have been carried out here at various temperatures, and we have estimated both  $T_\theta$  and  $b_k$ , it is possible to calculate  $v(T)$  in both good and poor solvents using Eqs. (6) to (8). As a result the size of a thermal blob as a function of temperature can also be estimated.

The equations that govern the dimensionless excluded volume parameter  $v_0/b_k^3$  and the molecular weight  $M_{\text{blob}}$  of a chain segment within a thermal blob, in good and poor solvents, are tabulated in Table I, when the hydrodynamic radius  $R_H$  is used as a measure of chain size. Here,  $m_k$  is the molar mass of a Kuhn-step, and the universal amplitude ratio  $U_R$  has been used to relate the mean size  $R$  to  $R_g$  ( $R = U_R R_g$ ), while the universal ratio  $U_{RD}$  relates  $R_g$  to  $R_H$  ( $R_g = U_{RD} R_H$ ). The values of these ratios are known analytically for the

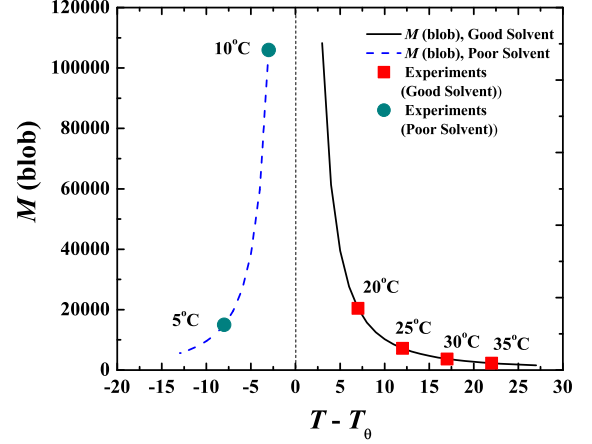


FIG. 15. Variation of the molecular weight of the chain segment within a thermal blob with respect to temperature, on either side of the  $\theta$ -temperature, in Solvent I (see Table I for the equations governing  $M_{\text{blob}}$ ). The symbols denote values at temperatures at which experimental measurements have been made.

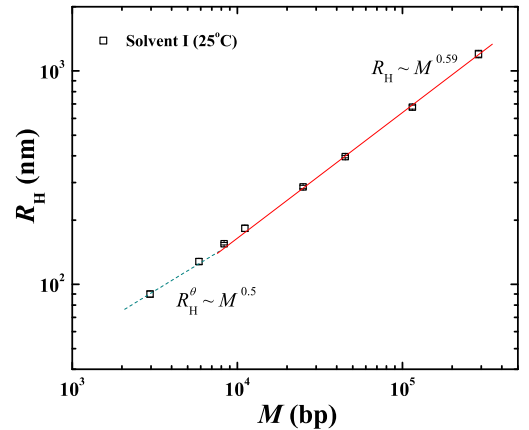


FIG. 16. The variation of hydrodynamic radius ( $R_H$ ) with molecular weight (in bp) in Solvent I, at 25°C.

case of Gaussian chains and Zimm hydrodynamics under  $\theta$ -conditions<sup>63</sup>, and numerically in the case of good solvents<sup>47</sup> and fluctuating hydrodynamic interactions<sup>59</sup>.

Using the known values of  $a$ ,  $\Pi_H$ ,  $b_k$ ,  $m_k$ ,  $U_{RD}$ ,  $U_R$  in the appropriate equations in Table I, we find that for sufficiently high molecular weights,  $v_0/b_k^3 \approx 4.7 \pm 0.5$  in Solvent I, while  $v_0/b_k^3 \approx 11 \pm 1$  in Solvent II, in both good and poor solvents. This is significant since an inaccurate measurement of mean size in a poor solvent (as a consequence of, for instance, chain aggregation), would result in different values of  $v_0/b_k^3$  in good and poor solvents. Further evidence regarding the reliability of poor solvent measurements can be obtained by calculating  $M_{\text{blob}}(T)$  in good and poor solvents.



solvent quality	good	poor
$\frac{v_0}{b_k^3}$ (for $M > M_{\text{blob}}$ )	$\left[ \frac{a \Pi_H (U_R U_{RD}) m_k^v}{b_k} \right]^{\frac{1}{2v-1}} \frac{1}{M^{\frac{1}{2}} \left( 1 - \frac{T_\theta}{T} \right)}$	$\left[ \frac{a \Pi_H (U_R U_{RD})}{b_k} \right]^{-3} \frac{1}{m_k M^{\frac{1}{2}} \left( 1 - \frac{T}{T_\theta} \right)}$
$M_{\text{blob}}(T)$	$\frac{m_k b_k^6}{v_0^2 \left( 1 - \frac{T_\theta}{T} \right)^2}$	$\frac{m_k b_k^6}{v_0^2 \left( 1 - \frac{T}{T_\theta} \right)^2}$

TABLE I. Equations for the dimensionless excluded volume parameter  $v_0/b_k^3$ , and the molecular weight of the chain segment within a thermal blob  $M_{\text{blob}}$ , in good and poor solvents. Here,  $m_k$  is the molar mass of a Kuhn-step, and  $U_R$  and  $U_{RD}$  are universal amplitude ratios, such that  $R = U_R R_g$ , and  $R_g = U_{RD} R_H$ .

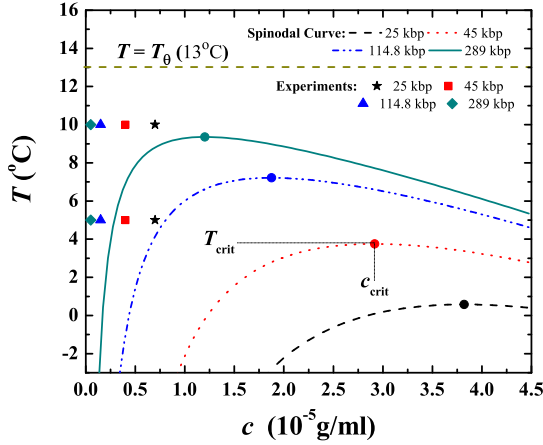


FIG. 17. Spinodal curves and critical temperatures and concentrations (filled circles) predicted by Flory-Huggins mean-field theory for a range of molecular weights in Solvent I. Values of concentrations and temperatures at which the poor solvent experiments have been conducted are also indicated.

Figure 15 displays the variation of  $M_{\text{blob}}$  with respect to the temperature difference  $T - T_\theta$  in Solvent I, calculated using the equations given in Table I. The figure graphically demonstrates the temperature dependence of the blob size, and confirms that essentially the blob size is the same in either a good or poor solvent when the temperature is equidistant from the  $\theta$ -temperature. The symbols in Fig. 15 denote values of  $M_{\text{blob}}$ , evaluated at the temperatures at which experimental measurements have been made. These values have been represented by the filled red circles in Fig. 14. As can be seen from Fig. 14, the magnitude of  $M_{\text{blob}}$  is roughly consistent with the location of the crossover from the scaling regime within a blob, to the scaling regime that holds at length scales larger than the blob, in both good and poor solvents. The two scaling regimes, at 25°C in Solvent I, are illustrated explicitly in Fig. 16.

The possibility of phase separation under poor solvent conditions, as polymer-solvent interactions become less favourable, is the primary reason for the difficulty of accurately measuring the size scaling of single chains. An approx-

imate estimate of the thermodynamic driving force for phase separation can be obtained with the help of Flory-Huggins mean field theory. Since the Flory-Huggins  $\chi$  parameter is related to the excluded volume parameter through the relation<sup>34</sup>  $\chi = \frac{1}{2} \left( 1 - \frac{v_0}{b_k^3} \right)$ , and we have estimated the value of

$v_0/b_k^3$  in both solvents, the phase diagram predicted by Flory-Huggins theory for dilute DNA solutions considered here can be obtained. It is appropriate to note that we are not interested in accurately mapping out the phase diagram for DNA solutions with the help of Flory-Huggins theory. This has already been studied in great detail, using sophisticated versions of mean-field theory, starting with the pioneering work of Post and Zimm<sup>64</sup>, and the problem of DNA condensation is an active field of research<sup>65–67</sup>. Our primary interest is to obtain an approximate estimate of the location of the current experimental measurements relative to the unstable two-phase region (whose boundary is determined by the spinodal curve), since phase separation can occur spontaneously within this region. Figure 17 displays the spinodal curves for the 25 to 289 kbp molecular weight samples in Solvent I, predicted by Flory-Huggins theory. Details of how these curves can be obtained are given, for instance, in Rubinstein and Colby<sup>34</sup>. Also indicated on each curve are the critical concentration and temperature. It is clear by considering the location of the symbols denoting the concentration-temperature coordinates of the poor solvent experiments, that for each molecular weight, they are located outside the unstable two-phase region, lending some justification to the reliability of the present poor solvent measurements. It is appropriate to note here that mean-field theories do not accurately predict the shape of the binodal curve, and in general concentration fluctuations tend to make the curve wider close to the critical point<sup>34</sup>. Interestingly, even for the 289 kbp sample, that has a very large molecular weight ( $\approx 1.9 \times 10^8$  Dalton), there is still a considerable gap between the critical and  $\theta$ -temperatures ( $\approx 4^\circ\text{C}$ ). The reason for this is because the stiffness of double-stranded DNA leads to a relatively small number of Kuhn-steps (1120) even at this large value of molecular weight, and the value of the critical temperature predicted by Flory-Huggins theory depends on the number of Kuhn-steps in a chain rather than the molecular weight.

#### IV. CONCLUSION

Static and dynamic properties of DNA in two commonly used buffer solutions have been characterized in terms of parameters used in dilute polymer solution theory. Using known scaling relationships from polymer solution theory, the  $\theta$ -temperatures ( $T_\theta$ ) in each of the solvents and the cross over of the swelling of the two radii in good solvent conditions ( $T > T_\theta$ ) were determined. DNA in Solvent I (10 mM Tris, 1 mM EDTA, 0.5 M NaCl) has  $T_\theta = 13 \pm 2$  °C and DNA in Solvent II (10 mM Tris, 1 mM EDTA, 0.5 M NaCl with 61.2 wt.% Sucrose) has  $T_\theta = 23 \pm 2$  °C. As with the regular polymers, the cross-over data of DNA can also be collapsed into a unique function of a scaling variable  $z = k(1 - T_\theta/T) \sqrt{M}$ . This confirms the two parameter theory hypothesis for DNA, that the static and dynamic properties of DNA in these good solvents can be uniquely determined from just two parameters: Radius of gyration at  $T_\theta$  ( $R_g^\theta$ ) and the solvent quality  $z$ . The scaling functions also agree within experimental error with the functions for synthetic polymers and model chains in good solvents obtained using molecular simulations. The results obtained here enable the determination of the solvent quality of DNA solutions, and consequently, facilitate the prediction of the behaviour of DNA molecules under various types of flows and geometrical constraints through molecular simulations or other theoretical approaches.

#### ACKNOWLEDGMENTS

We are grateful to Douglas E. Smith and his group in University of California (San Diego, USA) for preparing the majority of the special DNA fragments and to Brad Olsen, MIT (Cambridge, USA) for the stab cultures containing them. We thank Santosh Noronha and his group (IIT Bombay, India) for helpful discussions, laboratory support, and the two plasmids, pBSKS and pHCMC05, used in this work. JRP gratefully acknowledges very helpful discussions with Burkhard Dünweg. We also acknowledge the funding received from DST, DBT, and MHRD and IITB-Monash Research Academy. The Sophisticated Analytical Instrument Facility (SAIF), IIT Bombay is thanked for access to the static light scattering facility.

See supplementary material at [URL to be inserted by AIP] for details of strains and working conditions; procedures for preparation of linear DNA fragments; solvent composition and quantification of DNA samples; procedure for sample preparation for light scattering; methodology for measuring gyration and hydrodynamic radii, and the approach used here for determining second virial coefficients.

<sup>1</sup>J.-L. Barrat and J.-F. Joanny, *Adv. Chem. Phys.* **94** (XCIV), 1 (1996).

<sup>2</sup>D. E. Smith, T. T. Perkins, and S. Chu, *Macromolecules* **29**, 1372 (1996).

<sup>3</sup>S. S. Sorlie and R. Pecora, *Macromolecules* **23**, 487 (1990).

<sup>4</sup>R. M. Robertson, S. Laib, and D. E. Smith, *Proc. Natl. Acad. Sci. U. S. A.* **103**, 7310 (2006).

<sup>5</sup>J. F. Marko and E. D. Siggia, *Macromolecules* **28**, 8759 (1995).

<sup>6</sup>C. Bustamante, J. F. Marko, E. D. Siggia, and S. Smith, *Science* **265**, 1599 (1994).

<sup>7</sup>R. Pecora, *Science* **251**, 893 (1991).

<sup>8</sup>P. Sunthar and J. R. Prakash, *Macromolecules* **38**, 617 (2005).

<sup>9</sup>D. E. Smith and S. Chu, *Science* **281**, 1335 (1998).

<sup>10</sup>P. Sunthar, D. A. Nguyen, R. Dubbelboer, J. R. Prakash, and T. Sridhar, *Macromolecules* **38**, 10200 (2005).

<sup>11</sup>S. Laib, R. M. Robertson, and D. E. Smith, *Macromolecules* **39**, 4115 (2006).

<sup>12</sup>F. Valle, M. Favre, P. De Los Rios, A. Rosa, and G. Dietler, *Phys. Rev. Lett.* **95**, 1 (2005).

<sup>13</sup>D. E. Smith, T. T. Perkins, and S. Chu, *Macromolecules* **29**, 1372 (1996).

<sup>14</sup>I. Nayvelt, T. Thomas, and T. J. Thomas, *Biomacromolecules* **8**, 477 (2007).

<sup>15</sup>D. A. Ostrander and H. B. Gray Jr, *Biopolymers* **12**, 1387 (1973).

<sup>16</sup>P. D. Ross and R. L. Scruggs, *Biopolymers - Peptide Science Section* **6**, 1005 (1968).

<sup>17</sup>J. L. Hodnett, R. J. Legerski, and H. B. Gray Jr, *Anal. Biochem.* **75**, 522 (1976).

<sup>18</sup>M. A. Sibileva, A. N. Veselkov, S. V. Shilov, and E. V. Frisman, *Molekul-yarnaya Biologiya* **21**, 647 (1987).

<sup>19</sup>V. M. Marathias, B. Jerkovic, H. Arthanari, and P. H. Bolton, *Biochemistry* **39**, 153 (2000).

<sup>20</sup>T. Nicolai and M. Mandel, *Macromolecules* **22**, 2348 (1989).

<sup>21</sup>B. S. Fujimoto, J. M. Miller, N. S. Ribeiro, and J. M. Schurr, *Biophys. J.* **67**, 304 (1994).

<sup>22</sup>S. B. Leighton and I. Rubenstein, *J. Mol. Biol.* **46**, 313 (1969).

<sup>23</sup>P. Doty, B. B. McGill, and S. A. Rice, *Proc. Natl. Acad. Sci. U. S. A.* **44**, 432 (1958).

<sup>24</sup>J. Selis and R. Pecora, *Macromolecules* **28**, 661 (1995).

<sup>25</sup>D. M. Fishman and G. D. Patterson, *Biopolymers* **38**, 535 (1996).

<sup>26</sup>J. Langowski, U. Giesen, and C. Lehmann, *Biophys. Chem.* **25**, 191 (1986).

<sup>27</sup>G. Chirico, P. Crisafulli, and G. Baldini, *Il Nuovo Cimento D* **11**, 745 (1989).

<sup>28</sup>J. Langowski, *Biophys. Chem.* **27**, 263 (1987).

<sup>29</sup>Y. Liu, Y. Jun, and V. Steinberg, *J. Rheol.* **53**, 1069 (2009).

<sup>30</sup>J. S. Hur, E. S. G. Shaqfeh, H. P. Babcock, D. E. Smith, and S. Chu, *J. Rheol.* **45**, 421 (2001).

<sup>31</sup>C. M. Schroeder, H. P. Babcock, E. S. G. Shaqfeh, and S. Chu, *Science* **301**, 1515 (2003).

<sup>32</sup>H. P. Babcock, R. E. Teixeira, J. S. Hur, E. S. G. Shaqfeh, and S. Chu, *Macromolecules* **36**, 4544 (2003).

<sup>33</sup>M. J. Kim and I. H. Park, *Bull. Korean Chem. Soc.* **22**, 1255 (2001).

<sup>34</sup>M. Rubinstein and R. H. Colby, *Polymer Physics* (Oxford University Press, 2003).

<sup>35</sup>R. C. Hayward and W. W. Graessley, *Macromolecules* **32**, 3502 (1999).

<sup>36</sup>H. Yamakawa, *Modern Theory of Polymer Solutions*, electronic ed. (Kyoto University (formerly by Harper and Row), Kyoto, 2001).

<sup>37</sup>Y. Miyaki and H. Fujita, *Macromolecules* **14**, 742 (1981).

<sup>38</sup>L. Schäfer, *Excluded Volume Effects in Polymer Solutions* (Springer-Verlag, Berlin, 1999).

<sup>39</sup>K. S. Kumar and J. R. Prakash, *J. Chem. Phys.* **121**, 3886 (2004).

<sup>40</sup>J. R. Prakash, *J. Rheol.* **46**, 1353 (2002).

<sup>41</sup>J. Sambrook and D. W. Russell, *Molecular Cloning: A Laboratory Manual* (3rd edition) (Cold Spring Harbor Laboratory Press, USA, 2001).

<sup>42</sup>K. Soda and A. Wada, *Biophys. Chem.* **20**, 185 (1984).

<sup>43</sup>H. Liu, J. Gapinski, L. Skibinska, A. Patkowski, and R. Pecora, *J. Chem. Phys.* **113**, 6001 (2000).

<sup>44</sup>W. R. Krigbaum, *J. Am. Chem. Soc.* **76**, 3758 (1954).

<sup>45</sup>T. A. Orofino and J. W. Mickey Jr, *J. Chem. Phys.* **38**, 2512 (1963).

<sup>46</sup>A. R. Shultz and P. J. Flory, *J. Am. Chem. Soc.* **74**, 4760 (1952).

<sup>47</sup>K. S. Kumar and J. R. Prakash, *Macromolecules* **36**, 7842 (2003).

<sup>48</sup>V. Rizzo and J. Schellman, *Biopolymers* **20**, 2143 (1981).

<sup>49</sup>K. L. Cairney and R. E. Harrington, *Biopolymers* **21**, 923 (1982).

<sup>50</sup>G. Maret and G. Weill, *Biopolymers* **22**, 2727 (1983).

<sup>51</sup>C. G. Baumann, S. B. Smith, V. A. Bloomfield, and C. Bustamante, *Proc. Natl. Acad. Sci. U. S. A.* **94**, 6185 (1997).

<sup>52</sup>J. R. Wenner, M. C. Williams, I. Rouzina, and V. A. Bloomfield, *Biophys. J.* **82**, 3160 (2002).

<sup>53</sup>E. S. Sobel and J. A. Harpst, *Biopolymers* **31**, 1559 (1991).

<sup>54</sup>Z. Kam, N. Borochoy, and H. Eisenberg, *Biopolymers* **20**, 2671 (1981).

<sup>55</sup>N. Borochoy, H. Eisenberg, and Z. Kam, *Biopolymers* **20**, 231 (1981).

<sup>56</sup>G. Manning, *Biopolymers* **20**, 1751 (1981).

- <sup>57</sup>J. M. Schurr and S. A. Allison, *Biopolymers* **20**, 251 (1981).
- <sup>58</sup>P. J. Hagerman, *Annual review of biophysics and biophysical chemistry* **17**, 265 (1988).
- <sup>59</sup>P. Sunthar and J. R. Prakash, *Europhys. Lett.* **75**, 77 (2006).
- <sup>60</sup>Y. Tominaga, I. I. Suda, M. Osa, T. Yoshizaki, and H. Yamakawa, *Macromolecules* **35**, 1381 (2002).
- <sup>61</sup>A. J. Barrett, M. Mansfield, and B. C. Benesch, *Macromolecules* **24**, 1615 (1991).
- <sup>62</sup>C. Domb and A. J. Barrett, *Polymer* **17**, 179 (1976).
- <sup>63</sup>M. Doi and S. F. Edwards, *The Theory of Polymer Dynamics* (Clarendon Press, Oxford, New York, 1986).
- <sup>64</sup>C. B. Post and B. H. Zimm, *Biopolymers* **21**, 2123 (1982).
- <sup>65</sup>K. Yoshikawa, M. Takahashi, V. Vasilevskaya, and A. Khokhlov, *Phys. Rev. Lett.* **76**, 3029 (1996).
- <sup>66</sup>Y. Yoshikawa, Y. Suzuki, K. Yamada, W. Fukuda, K. Yoshikawa, K. Takeyasu, and T. Imanaka, *J. Chem. Phys.* **135**, 225101 (2011).
- <sup>67</sup>V. B. Teif and K. Bohinc, *Prog. in Biophys. and Mol. Biol.* **105**, 208 (2011).

# Supplementary material for: Polymeric Behaviour of DNA: Theta Temperature and Good Solvent Cross-over of Gyration and Hydrodynamic Radii

Sharadwata Pan,<sup>1,2,3</sup> P. Sunthar,<sup>2,1</sup> T. Sridhar,<sup>3,1</sup> and J. Ravi Prakash<sup>3,1, a)</sup>

<sup>1)</sup>IITB-Monash Research Academy, Indian Institute of Technology Bombay, Powai, Mumbai - 400076, India

<sup>2)</sup>Department of Chemical Engineering, Indian Institute of Technology Bombay, Powai, Mumbai - 400076, India

<sup>3)</sup>Department of Chemical Engineering, Monash University, Melbourne, VIC 3800, Australia

(Dated: 11 May 2019)

## I. DETAILS OF STRAINS, WORKING CONDITIONS AND PROCEDURES FOR PREPARING LINEAR DNA FRAGMENTS.

Recently, a range of special DNA constructs, from 3 – 300 kbp, have been genetically engineered into bacterial strains of *E. coli*<sup>1</sup>, which can be selectively extracted for rheological studies. Primarily they fall into three categories: plasmids, fosmids and Bacterial Artificial Chromosomes (BAC). Altogether six samples (two plasmids, two fosmids and two BACs), which were originally prepared elsewhere<sup>1</sup> were procured from Dr. Brad Olsen, California Institute of Technology, USA. Throughout the work, the nomenclature of all the three types of DNA samples has been used as in the originally published work<sup>1</sup>. In addition, two special bacterial strains containing the plasmids: pBSKS (2.7 kbp) and pHCMC05 (8.3 kbp) were provided by Dr. S. Noronha, Dept. of Chemical Engineering, IIT Bombay (India). The details about size, growth conditions of bacteria and single cutters of the DNA samples are mentioned in Table I. After procurement of samples (in the form of agar stab cultures of *E. coli*), glycerol freeze stocks were made using 50% glycerol and stored at -80°C. The cultures can be stored in this way for several years and can be used at any time to produce DNA samples<sup>1</sup>.

Standard procedures<sup>1,2</sup> involving alkaline lysis (mediated by NaOH) were adopted for extraction, linearization and purification of plasmids, fosmids and BAC from the cultures. For high copy number plasmids, no inducer was added. For low (fosmids) and very low (BACs) copy number samples, L-arabinose was added as inducer. From each freeze stock, 15 $\mu$ l of ice was scrapped and transferred to 40 ml LB medium with proper antibiotic (as mentioned in Table I) and incubated overnight (16 – 18 hours) at 37°C with vigorous shaking (200 – 250 rpm). The overnight grown culture was poured into microcentrifuge tubes and cells were harvested by centrifugation. The bacterial pellet (obtained above) was resuspended in 100 $\mu$ l of ice-cold Solution I (4°C)<sup>2</sup> followed by 200 $\mu$ l of freshly prepared Solution II<sup>2</sup> and 150 $\mu$ l of ice-cold Solution III<sup>2</sup>. The tubes were stored on ice for 3–5 minutes and centrifuged. The supernatant was transferred to a fresh tube. The precipitate (containing mainly the cell debris and genomic DNA) was discarded. RNase was added (at 10  $\mu$ g/ml) to the

tube and incubated at 37°C for 20 minutes. Equal volume of Phenol-Chloroform-Isoamyl Alcohol (25:24:1) mixture was added and mixed well by vortexing. After centrifugation, supernatant was transferred to a fresh tube. Equal volume of Chloroform was added and centrifuged. The supernatant was transferred to a fresh tube. Two volumes of chilled 100% ethanol (at 4°C) was added at room temperature kept for 7–8 hours at -20°C. The tube was then centrifuged and the supernatant removed by gentle aspiration. The tube was kept in an inverted position in a paper towel to allow all of the fluid to drain away. Following this, 1 ml of 70% ethanol was added to the tube and centrifuged. When all of the ethanol was evaporated, the resulting DNA pellet was dissolved in 50 $\mu$ l of Milli-Q grade water and stored at -20°C.

To linearize the extracted DNA fragments, 39 $\mu$ l of water was added to a 1.7 ml microcentrifuge tube, followed by 10 $\mu$ l of corresponding 10X Assay Buffer (working concentration is 1X) and 50 $\mu$ l of DNA solution (purified DNA stored at 4°C). 1  $\mu$ l of appropriate enzyme was added. A thumb rule is 0.5 - 1 U enzyme for 1 mg DNA<sup>2</sup>. The samples were mixed well with micropipette (wide bore tips) for several times. The reaction mix (100 $\mu$ l) was incubated at 37°C for three hours. After restriction digestion / linearization, it is necessary to remove the enzymes / other reagents present in the reaction mix so that they do not interfere with the downstream application/s like light scattering studies, rheometry etc. For this normal phenol-chloroform extraction followed by ethanol precipitation of DNA was carried out as described elsewhere<sup>2</sup>.

## II. SOLVENTS I AND II

Two different solvents were used in this study (see Table II). Solvent I is primarily the widely used Tris-EDTA buffer, supplemented with 0.5 M NaCl. Solvent II is the same but with added sucrose (61.2 wt.%), mainly to increase the viscosity by approximately 60 times. The measured viscosities of Solvent I and Solvent II at 20°C are 1.01 and 58 mPa-s respectively.

## III. QUANTIFICATION OF DNA SAMPLES

After the DNA samples were extracted and purified, their purity were determined using the Nano-Photometer (UV-VIS Spectrophotometer, IMPLN, Germany). Optical Density

<sup>a)</sup>Corresponding author: ravi.jagadeeshan@monash.edu

TABLE I. DNA Fragments. Here 'LB' stands for Luria Bertini broth, 'Ant<sup>R</sup>' refers to Antibiotic resistance, 'Amp.' refers to Ampicillin, 'CAM' refers to Chloramphenicol, 'Kan' refers to Kanamycin, all the cultures were incubated overnight at 37°C with vigorous shaking (200–250 rpm). L-arabinose (inducer) was used at a concentration of 0.01g per 100 ml (stock concentration: 5g in 100ml). Stock concentrations for preparations of Ampicillin, Chloramphenicol and Kanamycin were 100 mg/ml, 25 mg/ml and 100 mg/ml respectively. The working concentrations for Amp., CAM and Kan are 100 µg/ml, 12.5µg/ml and 100µg/ml respectively. Growth conditions for all the plasmids are same (LB + Amp.) except pHCMC05 (LB + Amp. + CAM). For both the fosmids, growth conditions are identical (LB + CAM + L-arabinose). For both the BACs, growth conditions are same (LB + CAM + Kan + L-arabinose).

Type	Name	Size (kb) / (Notation)	Ant <sup>R</sup>	I Cutter
Plasmid	pBSKS(+)	2.9 / F2.9	Amp.	BamHI
	pYES2	5.9 / F5.9	Amp.	BamHI
	pHCMC05	8.3 / F8.3	Amp. + CAM	BamHI
	pPIC9K<TRL5>	11.1 / F11.1	Amp.	
Fosmid	pCC1FOS-25	25 / F25	CAM	Apal
	pCC1FOS-45	45 / F45	CAM	Apal
BAC	CTD-2342K16	114.8 / F114.8	CAM + Kan	MluI
	CTD-2657L24	289 / F289	CAM + Kan	MluI

TABLE II. Composition of Solvents used in the study.

Solvent I	Solvent II
10 mM Tris	10 mM Tris
1 mM EDTA	1 mM EDTA
0.5 M NaCl	0.5 M NaCl
Water	61.2 wt% Sucrose Water

(O.D.) readings were taken at three different wavelengths: 260 nm, 280 nm and 230 nm. The ratio of absorbance at 260 nm to that of 280 nm gives a rough indication of DNA purity<sup>2</sup>. The concentrations were calculated from absorbance reading at 260 nm (DNA shows absorption peak at 260 nm) by Beer-Lambert's Law<sup>2</sup> and also by agarose gel electrophoresis through a serial dilution of DNA samples as suggested elsewhere<sup>1</sup>. All the linear DNA samples demonstrated  $A_{260}/A_{280}$  ratio of 1.8 and above. This indicates good purity for DNA samples, though it is largely an assumption<sup>1</sup> and  $A_{260}/A_{230}$  ratio from 2.0 to 2.2 (absence of organic reagents like phenol, chloroform etc)<sup>1</sup>. The low molecular weight linear DNA fragments (plasmids) were quantified through agarose gel electrophoresis with a known standard 1 kbp DNA marker (Fermentas). For low copy number fragments (fosmids) and very low copy number samples (BACs), it was confirmed that the samples were not sheared during extraction by running a very low concentration agarose gel for extended period at low voltage. A loss of 25% – 50% was observed in the amount of DNA samples after the linearization procedure. This is attributed to purification steps by phenol-chloroform extraction<sup>2</sup>.

#### IV. SAMPLE PREPARATION FOR LIGHT SCATTERING

All the linear DNA fragments were dissolved individually in both the solvents and were characterized by dynamic light scattering (DLS) for the hydrodynamic radius,  $R_H$  and by static light scattering (SLS) for the radius of gyration,  $R_g$ . For

TABLE III.  $c^*$  values (in µg/ml) for different DNA fragments used in this study in Solvent I at different temperatures.

Size (kbp)	15°C	20°C	25°C	30°C	35°C
2.9	353	323	295	241	210
5.9	244	231	210	154	141
8.3	198	187	163	124	104
11.1	172	152	129	103	84
25	110	90	75	60	53
45	68	51	39	34	28
114.8	31	22	15	12	10
289	16	8	5	4	3

both dynamic and static light scattering, an extensive sample preparation method was followed to ensure repeatability. The methodology of sample preparation was modified from earlier studies<sup>3–5</sup> and was repeated before each measurement. The cuvette was washed with ethanol (0.5 ml) for 5 times and kept for 15 minutes inside laminar air flow. It was followed by wash with milliQ grade water for 10 – 15 minutes continuously. In the meantime, the solvents were filtered with 0.45µ membrane-filter (PALL Corp.,USA) with 2 different membranes consecutively. After filtration, DNA was added to make final concentration of  $c/c^* = 0.1$  (for DLS) and  $c/c^* = 0.05 - 0.1$  (for SLS). The  $c^*$  values for different DNA fragments used in this study in Solvent I at different temperatures are summarized in Table III.

#### V. CHARACTERIZATION OF LINEAR DNA SAMPLES

Dynamic Light Scattering was used for measuring the hydrodynamic radii of all the molecular weights at different temperatures: 5°C, 10°C, 15°C, 20°C, 25°C, 30°C and 35°C in Solvent I and 10°C, 15°C, 20°C, 25°C, 30°C and 35°C in Solvent II. Static Light Scattering was used for measuring the radii of gyration of all the molecular weights at different temperatures: 15°C, 20°C, 25°C, 30°C and 35°C in both Solvents I and II. Static Light Scattering was also used to find out the

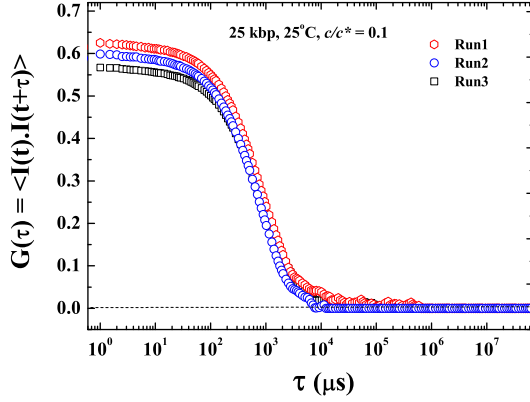


FIG. 1. Intensity autocorrelation spectra for 25 kbp DNA at 25°C and  $c/c^* = 0.1$ .

second virial coefficients at different temperatures: 11.2°C, 13°C, 14°C, 15°C and 20°C in Solvent I and 19°C, 21°C, 23°C and 25°C in Solvent II.

## VI. DYNAMIC LIGHT SCATTERING: TAKING MEASUREMENTS

The dynamic size characterization of dilute DNA solutions was done using a Zetasizer Nano ZS (ZEN3600, MALVERN, U.K.) particle size analyzer with temperature control fitted with a 633 nm He-Ne laser using back-scattering detection. This instrument uses dynamic light scattering (or quasi-elastic light scattering / photon correlation spectroscopy) to measure the diffusion coefficient which is then converted to an average hydrodynamic size of particles in solution using the Stokes-Einstein equation. A Standard Operating Procedure (SOP) was created using the Dispersion Technology Software (DTS 5.00, MALVERN, U.K.) to achieve the desired outcome ( $R_H$ ) without manual intervention. Scattering of the DNA solutions was measured at a fixed 173° scattering angle (this enables measurements even at high sample concentrations and the effect of dust is greatly reduced). The temperature range investigated was from 5 to 35°C for Solution I and 10 to 35°C for Solution II. A typical example of measured intensity autocorrelation spectra for 25 kbp DNA at 25°C and  $c/c^* = 0.1$  is shown in Figure 1. Note that,  $G(\tau) = \langle I(t)I(t + \tau) \rangle$ , where  $I$  is the intensity of scattered light, and  $\tau$  is the time difference of the correlator. The Zetasizer Nano ZS has the ability to measure a wide size range (0.6–6000 nm in diameter). In this paper, we have reported sizes roughly in the range 140–4900 nm in diameter, which is within the size range of the instrument. Readings were taken in three temperature scans (a sequence of High-Low, Low-High, and High-Low temperature settings); with 5 readings at each temperature. The mean of 15 readings was taken as final data point at each temperature for each DNA fragment.

Measured values of  $R_H$  are reported in Tables IV and V.

TABLE IV. Hydrodynamic Radius ( $R_H$ ) of linear DNA at different temperatures in Solvent I. Each data point corresponds to the intensity peaks from DLS measurements. The mean of 15 readings was taken as final data point at each temperature for each DNA fragment.

Sequence length	2.9 kbp	5.9 kbp	8.3 kbp	11.1 kbp
Temperature	$R_H$ (in nm)	$R_H$ (in nm)	$R_H$ (in nm)	$R_H$ (in nm)
5°C	73±4	104±3	123±3	141±3
10°C	77±3	109±3	131±3	152±3
15°C	85±3	121±3	145±3	167±3
20°C	87±3	124±3	148±3	173±4
25°C	90±3	131±5	155±2	183±6
30°C	96±2	136±4	162±3	189±3
35°C	101±4	145±7	174±3	203±5

Sequence length	25 kbp	45 kbp	114.8 kbp	289 kbp
Temperature	$R_H$ (in nm)	$R_H$ (in nm)	$R_H$ (in nm)	$R_H$ (in nm)
5°C	203±4	258±5	385±13	540±35
10°C	226±5	303±6	473±14	718±46
15°C	258±3	349±4	560±18	897±57
20°C	267±8	367±4	607±13	1025±39
25°C	286±5	397±5	677±15	1201±49
30°C	297±4	417±6	722±13	1300±38
35°C	313±8	431±8	753±19	1363±57

TABLE V. Hydrodynamic Radius ( $R_H$ ) of linear DNA at different temperatures in Solvent II. Each data point corresponds to the intensity peaks from DLS measurements. The mean of 15 readings was taken as final data point at each temperature for each DNA fragment.

Sequence length	2.9 kbp	5.9 kbp	8.3 kbp	11.1 kbp
Temperature	$R_H$ (in nm)	$R_H$ (in nm)	$R_H$ (in nm)	$R_H$ (in nm)
10°C	150±15	194±17	213±16	223±14
15°C	152±15	209±16	242±13	267±17
20°C	160±5	234±9	265±8	305±10
25°C	167±6	236±8	282±7	327±8
30°C	175±9	248±7	298±6	346±6
35°C	181±8	256±5	305±3	354±4

Sequence length	25 kbp	45 kbp	114.8 kbp	289 kbp
Temperature	$R_H$ (in nm)	$R_H$ (in nm)	$R_H$ (in nm)	$R_H$ (in nm)
10°C	262±15	264±17		
15°C	349±10	396±13	528±21	613±30
20°C	455±6	609±10	954±11	1456±23
25°C	493±7	666±8	1072±9	1815±11
30°C	529±8	721±7	1214±5	2110±10
35°C	564±3	786±5	1345±5	2409±8

As expected, the hydrodynamic radius of DNA increases with both temperature and molecular weight, in both the solvents.

## VII. STATIC LIGHT SCATTERING: TAKING MEASUREMENTS

The static light scattering (SLS) measurements were obtained from a BI-200SM Goniometer (Brookhaven Instruments Corporation, USA) using BI-SLSW Static Light Scattering Software. A separate temperature control system

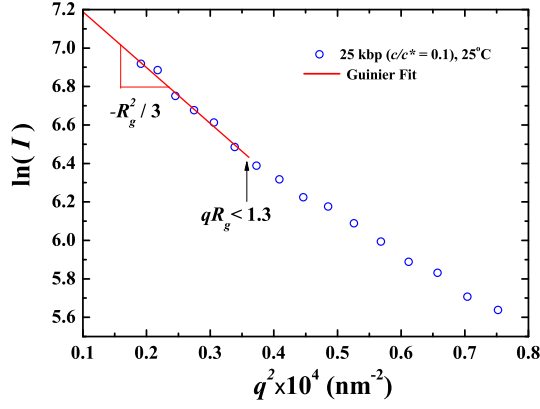


FIG. 2. Application of the Guinier approximation. Intensity as a function of scattering wave vector, measured for 25 kbp DNA at 25°C and  $c/c^* = 0.1$ .

(PolySc, USA) was arranged. For  $R_g$  measurements, the readings for each molecular weight were taken at different angles at different temperatures. The Guinier approximation for calculating  $R_g$  was employed. The angle range was selected based on sample concentration. A typical example of the application of the Guinier approximation for 25 kbp DNA at 25°C and  $c/c^* = 0.1$  is shown in Figure 2. The temperature range investigated was from 15 – 35°C (Solution I and Solution II). Readings were taken in two temperature scans; with 5 repeats at each temperature. The mean of 10 repeats was taken as final data point at each temperature for each DNA fragment. For determining the transition in the second virial coefficient (at the theta temperature), the intensity of scattered light was measured as a function of scattering vector (which is a function of the scattering angle) and DNA concentrations.  $R_g$  of the DNA increase with both temperature and molecular weight, in both solvents. This is reported in Tables VI and VII.

#### VIII. DETERMINATION OF SECOND VIRIAL COEFFICIENTS BY SLS

In this work, a single, linear, medium molecular weight DNA fragment (25 kbp) is taken and the intensity of scattered light,  $I_\theta$  is determined as a function of scattering vector,  $q^2$  and polymer concentration,  $c$  through SLS, at temperatures above and below the estimated  $\theta$ -point for the two systems. The readings from a typical plot of reciprocal scattering intensity ( $1/I_\theta$ ) against  $q^2$  (see Figure 3), are extrapolated to find the intensity at zero scattering angle ( $I_0$ ). For Solvent I, intensity readings are taken at 5 different temperatures between 10 – 20°C. For Solvent II, intensity readings are taken at 4 different temperatures between 20 – 25°C. Four different concentrations are used:  $c/c^* = 0.2, 0.3, 0.35$  and  $0.4$  ( $c^*$  is the overlap concentration, based on our measured  $R_g$ ). The second virial coefficients are determined according to a procedure described in Ref. 6. The dependence of reduced scattering ra-

TABLE VI. Radius of gyration ( $R_g$ ) of linear DNA fragments at different temperatures in TE Buffer (Solvent I). Each data corresponds to an average of 10 measurements performed in two temperature scans. The  $R_g$  values at  $T_\theta = 13^\circ\text{C}$  have been estimated by linear extrapolation of data points.

Sequence length	2.9 kbp	5.9 kbp	8.3 kbp	11.1 kbp
Temperature	$R_g$ (in nm)	$R_g$ (in nm)	$R_g$ (in nm)	$R_g$ (in nm)
13°C	125±2	174±4	206±5	234±9
15°C	129±2	184±5	221±7	255±6
20°C	133±5	187±8	225±8	266±9
25°C	137±6	193±5	236±4	281±8
30°C	147±3	214±4	258±2	303±7
35°C	154±3	220±5	274±4	324±9

Sequence length	25 kbp	45 kbp	114.8 kbp	289 kbp
Temperature	$R_g$ (in nm)	$R_g$ (in nm)	$R_g$ (in nm)	$R_g$ (in nm)
13°C	342±11	458±10	744±13	1212±37
15°C	389±6	554±15	980±22	1667±46
20°C	415±5	612±14	1098±24	2102±30
25°C	441±5	666±10	1242±23	2426±38
30°C	476±7	696±10	1347±17	2664±43
35°C	495±7	743±21	1415±32	2782±47

TABLE VII. Radius of gyration ( $R_g$ ) of linear DNA at different temperatures in Solvent II. Each data corresponds to an average of 10 measurements performed in two temperature scans. The  $R_g$  values at  $T_\theta = 23^\circ\text{C}$  have been estimated by linear interpolation of data points.

Sequence length	2.9 kbp	5.9 kbp	8.3 kbp	11.1 kbp
Temperature	$R_g$ (in nm)	$R_g$ (in nm)	$R_g$ (in nm)	$R_g$ (in nm)
15°C	162±5	226±9	269±14	308±16
20°C	166±2	238±9	286±12	328±10
23°C	173±4	245±10	297±11	350±13
25°C	178±1	252±4	305±4	373±11
30°C	187±2	267±4	327±12	387±13
35°C	194±6	275±9	341±10	412±17

Sequence length	25 kbp	45 kbp	114.8 kbp	289 kbp
Temperature	$R_g$ (in nm)	$R_g$ (in nm)	$R_g$ (in nm)	$R_g$ (in nm)
15°C	433±10	488±21	687±41	974±56
20°C	471±13	620±15	980±23	1486±71
23°C	525±12	690±16	1141±20	1845±40
25°C	564±12	788±16	1342±31	2317±66
30°C	620±11	892±19	1603±24	2681±59
35°C	679±15	948±21	1786±39	3059±80

tios at zero angle ( $c/I_0$ ) on the reduced concentration ( $c/c^*$ ) can be written as<sup>6</sup>:

$$(c/I_0)^{1/2} = (1/M)[1 + A_2(c/c^*) + A_3(c/c^*)^2 + \dots] \quad (1)$$

Here,  $M$  is Molecular Weight,  $A_2$  is second virial coefficient and  $A_3$  and subsequent coefficients resemble interaction terms of higher order. From the plots of  $(c/I_0)^{1/2}$  against  $c/c^*$  (see Figures 4 and 5), slopes ( $A_2/M$ ) are calculated at each temperature in accordance with Equation (1) by fitting the data points with straight lines and neglecting  $A_3$  and the other higher order coefficients.



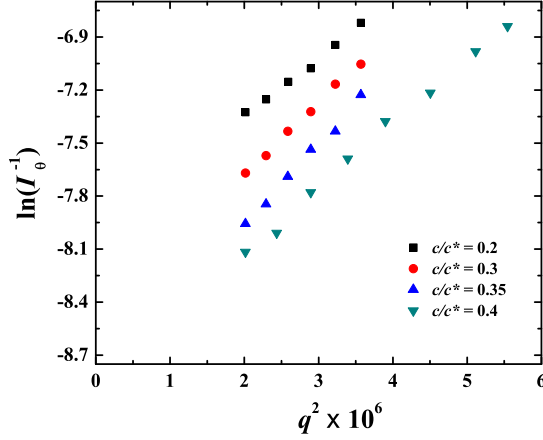


FIG. 3. Variation of reciprocal intensity for 25 kb linear DNA as a function of  $q^2$  (in Solvent I at 20°C). Here,  $q^2$  is a function of the scattering angle. The readings are extrapolated to find the intensity at zero scattering angle,  $I_0$ .

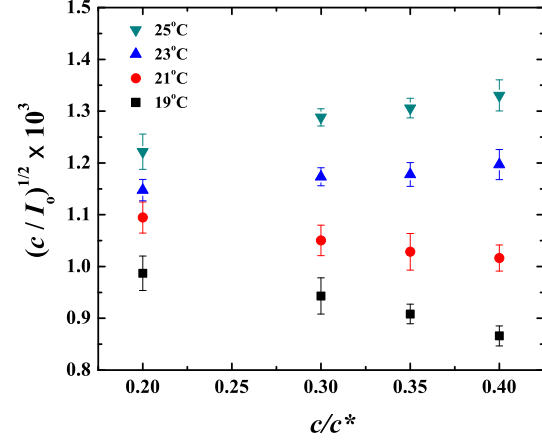


FIG. 5. Variation of reciprocal reduced intensity vs concentration (in Solvent II). Slopes are calculated at each temperature by linear fitting of the data points.

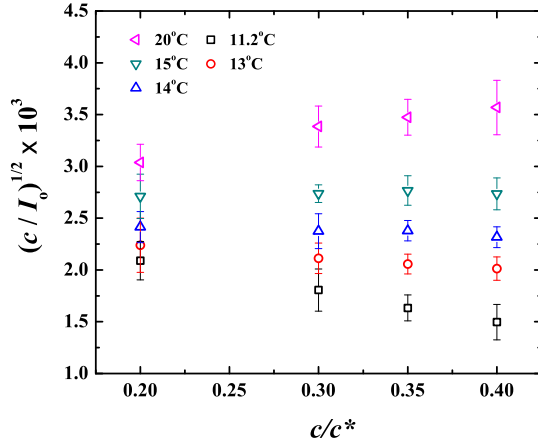


FIG. 4. Variation of reciprocal reduced intensity vs concentration (in Solvent I). Slopes are calculated at each temperature by linear fitting of the data points.

### IX. DETERMINATION OF THE CHEMISTRY DEPENDENT CONSTANT $k$ FOR SOLVENTS I AND II

The  $k$  values for both the solvents are determined by adopting a procedure elaborated in an earlier work<sup>7</sup>, and briefly summarised in the main text (see Section 3.2). Figure 6 displays plots of  $f_g^{-1}(\alpha_g^{\text{expt}})/\sqrt{M}$  versus  $\hat{\tau}$  for the two solvents. Only the temperatures above the theta point in both solvents are considered here. The data points were least square fitted with a straight line, and the slope  $k$  determined.  $\theta$ -temperature values of 13°C and 23°C have been used for Solvent I and II, respectively. The values of  $k$  found by this procedure are  $7.4 \times 10^{-3} \pm 3.0 \times 10^{-4}$  for Solvent I and  $5.5 \times 10^{-3} \pm 2.0 \times 10^{-4}$

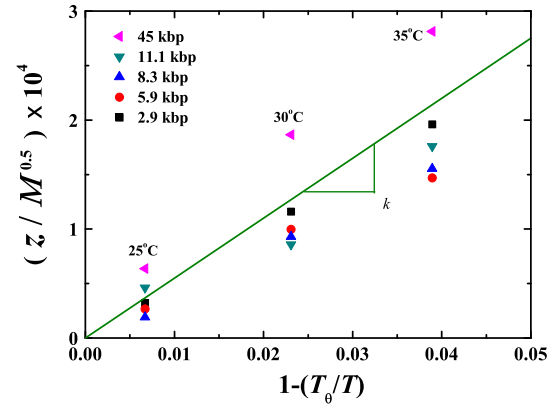
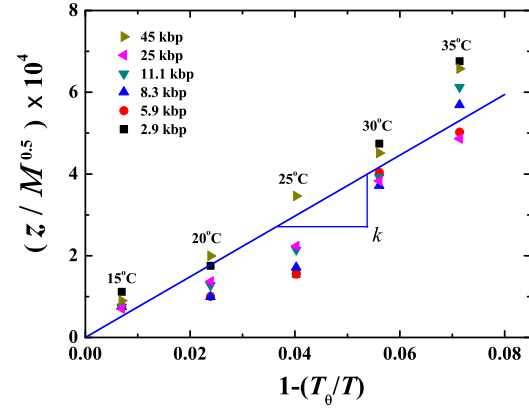


FIG. 6. Determination of  $k$  for (a) solvent I, and (b) solvent II. The data points (except 114.8 and 289 kbp) are least square fitted with a straight line and the slope of this line gives  $k^7$ .

for Solvent II. However, while estimating the value of  $k$ , very high molecular weight linear DNA fragments (114.8 and 289 kbp) in Solvent I and Solvent II were not considered, since they deviated from the general behaviour. The reason for this could be that at high temperatures (30°C and 35°C), the high molecular weight linear DNA chains swell profusely and may start overlapping with each other (in a crossover region between dilute and semi-dilute solutions) resulting in solutions that may not be dilute in a physical sense.

- <sup>1</sup>S. Laib, R. M. Robertson, and D. E. Smith, *Macromolecules* **39**, 4115 (2006).
- <sup>2</sup>J. Sambrook and D. W. Russell, *Molecular Cloning: A Laboratory Manual* (3rd edition) (Cold Spring Harbor Laboratory Press, USA, 2001).
- <sup>3</sup>S. S. Sorlie and R. Pecora, *Macromolecules* **23**, 487 (1990).
- <sup>4</sup>R. J. Lewis, J. H. Huang, and R. Pecora, *Macromolecules* **18**, 944 (1985).
- <sup>5</sup>J. Selis and R. Pecora, *Macromolecules* **28**, 661 (1995).
- <sup>6</sup>T. A. Orofino and J. W. Mickey Jr., *J. Chem. Phys.* **38**, 2512 (1963).
- <sup>7</sup>K. S. Kumar and J. R. Prakash, *Macromolecules* **36**, 7842 (2003).